Applied Catalysis B: Environmental 307 (2022) 121159

Contents lists available at ScienceDirect

Applied Catalysis B: Environmental

journal homepage: www.elsevier.com/locate/apcatb

Highly conductive $NiSe_2$ nanoparticle as a co-catalyst over TiO_2 for enhanced photocatalytic hydrogen production

S. Jayachitra [a,b,1], D. Mahendiran [a,b,2,3], P. Ravi [a,b,3,4], P. Murugan [a,b,*,5], M. Sathish [a,b,*,6]

[a] Electrochemical Power Sources Division, CSIR-Central Electrochemical Research Institute, Karaikudi 630003, Tamil Nadu, India
[b] Academy of Scientific and Innovative Research (AcSIR), Ghaziabad 201002, India

ARTICLE INFO

Keywords:
Photocatalyst
Supercritical fluid
Co-catalyst
Hydrogen evolution
Water splitting

ABSTRACT

Designing a photocatalyst for hydrogen production is pivotal role in renewable energy technologies. Herein, the synthesis of nanosized $NiSe_2$ particles via supercritical fluid process with the short reaction time of 30 min was reported. Then, it was used as a co-catalyst over TiO_2 to improve H_2 production rate. Supercritical fluid process is an effective and alternative technique for nanoparticle preparation in short time. In the presence of $NiSe_2$, the H_2 production rate of TiO_2 was greatly increased thereby attained the maximum activity of 219.2 mmol/h/g_{cat} with STH of 9% and is closer to that of Pt loaded TiO_2 (9.7% for 235.5 mmol/h/g_{cat}). The highly conductive nature of $NiSe_2$ facilitates rapid transfer of photogenerated electrons from TiO_2 to $NiSe_2$. The detailed possible mechanism was debated and confirmed by first principles DFT calculations. This work validates short time reaction to prepare highly conductive $NiSe_2$ as an electron sink for efficient H_2 production.

1. Introduction

The world has numerous energy resources among them fossil fuel are the major conventional sources of energy supply. However, its widespread usage results fast depletion because of population growth and increasing industrialization. Moreover, burning of fossil fuel emits lot of air pollutants, those are very harmful to human health. Of the many environmental problems associated with burning of fossil fuel, the most serious in terms of potentially irreversible impact is global warming. Hence, utilization of clean and sustainable energy system is one of the hopeful ways to make pollutant free environment, which reduces dependence on fossil fuel and also address the energy crisis, thereby creating economic development [1,2]. In that view, hydrogen energy is one of the green and sustainable fuel, having high energy density (120 MJ/Kg) which is almost three times more than gasoline [3,4]. Owing to this, the production of hydrogen from water splitting using solar energy has been widely studied [5]. Until now, many photocatalysts like TiO_2, g-C_3N_4, CdS, ZnS, ZnO, Cu_2O, Cu_2S, CdSe, NiO, ZnSe, and WO_3 have been studied for photocatalytic hydrogen production [6–11]. However, developing an effective photocatalyst with a suitable band edge position, low cost, non-toxic and more stable for sustainable water splitting reaction is still under challenge [12–15]. TiO_2 is regarded as benchmark material in the field of photocatalysis for pollutant removal. Although, its photocatalytic hydrogen production ability is highly restricted due to rapid recombination of photogenerated charge carriers and lack of visible light absorption [16–19]. To improve the photocatalytic efficiency, researchers have been developed various strategies like heterojunction, Z-scheme, co-catalyst, core-shell and formation of p-n junction using their unique properties [20–24]. One of the promising methods to develop the efficient photocatalytic hydrogen production is co-catalyst-based system [25–27]. In this aspect, best results have been attained by noble metals like Pt, Ir, Ru, and Rh, but because of their more expensive and low abundance in the earth crust, they were restricted for widespread implementation [28,29]. Many works have been focusing on finding a novel and noble metal free material as a co-catalyst to attain better rate of hydrogen production at economy level[30–32]. In recent

* Corresponding authors at: Electrochemical Power Sources Division, CSIR-Central Electrochemical Research Institute, Karaikudi 630003, Tamil Nadu, India.
E-mail addresses: murugan@cecri.res.in (P. Murugan), msathish@cecri.res.in (M. Sathish).
[1] 0000-0003-0400-6808.
[2] 0000-0003-4162-2300.
[3] Authors contributed equally to this work.
[4] 0000-0003-1254-8658.
[5] 0000-0002-6493-2283.
[6] 0000-0001-9094-5822.

https://doi.org/10.1016/j.apcatb.2022.121159
Received 10 November 2021; Received in revised form 11 January 2022; Accepted 28 January 2022
Available online 1 February 2022

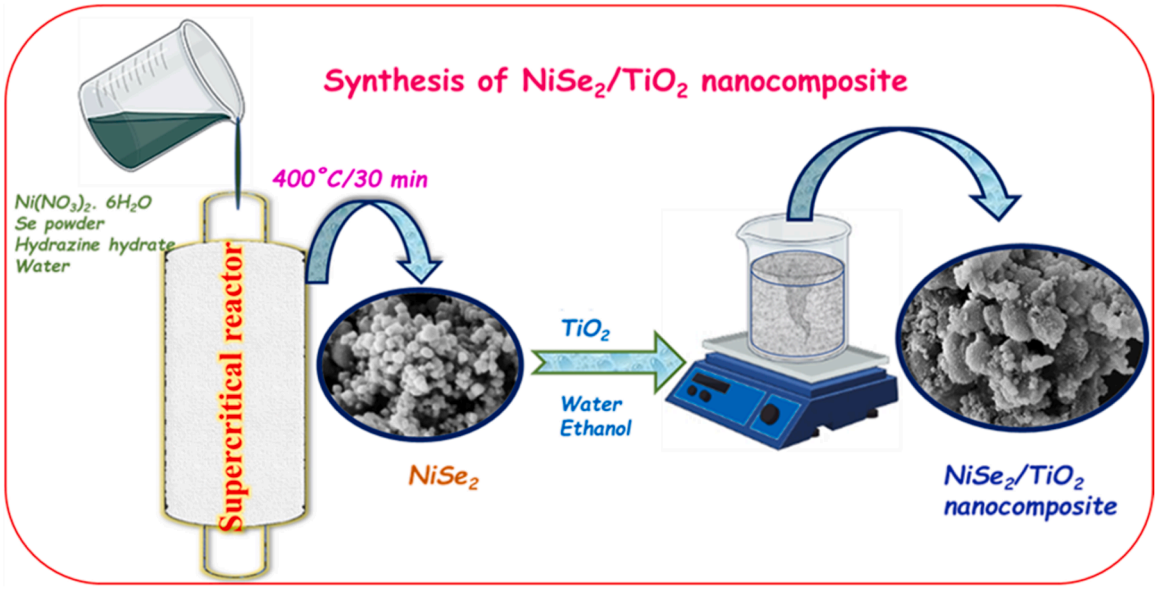

Scheme 1. Synthesis of $NiSe_2/TiO_2$ nanocomposite for photocatalytic hydrogen production.

years, metal chalcogenides are considered as a propitious candidate in the catalysis field because of their features like unique electronic, optical properties, low cost, and more abundant in the earth crust [33–35]. Particularly, metal selenides are superior one, because it possesses high electrical conductivity than respective oxides and sulfides due to metallic character of selenium. In this regard, fabrication of nickel-based selenides is very cheap and less toxic compare to cadmium and lead selenides. Furthermore, nickel-based selenides like Ni_3Se_2, Ni_3Se_4, $NiSe_2$, NiSe have been developed for several potential applications [36–39]. Among them, the $NiSe_2$ has been widely used in the field of solar cell, supercapacitor, water splitting, and also promising candidate for applications in sensor [40–42]. It also possesses an intrinsic electrical conductivity which can promote the conduction of electron, thereby it can be a suitable candidate for photocatalytic hydrogen generation. Owing to these considerations, it may be a sort of co-catalyst for overall water splitting with excellent performance. Over the last decades, Ni based selenides have been emerged as an active material for photocatalytic water splitting applications [43,44]. Recently, some studies have been reported on $NiSe_2$ for photocatalytic hydrogen production, such as $NiSe_2$/CdS nanocomposites for photocatalytic hydrogen production by Wang et al. [45], hierarchical 0D $NiSe_2$/2D $ZnIn_2S_4$ nanosheets for enhanced hydrogen evolution by Lai et al. [46], $Mn_{0.05}Cd_{0.95}S$ nanoparticles anchored on cubic $NiSe_2$ for efficient photocatalytic hydrogen production [47].

Here, at the first time the synthesis of $NiSe_2$ nanoparticles via supercritical fluid assisted method is reported, which has the advantages like one pot synthesis and short reaction time. For the preparation of $NiSe_2$ nanoparticles, water used as a solvent and the reaction time to form the desired product is 30 min. Then these nanoparticles are immobilized on the surface of TiO_2 nanoparticles to examine its effect during the photocatalytic water splitting reaction. Here, TiO_2 nanoparticles and $NiSe_2/TiO_2$ nanocomposite were prepared by sol-gel and wet impregnation method, respectively. And the formation of $NiSe_2$ integrated TiO_2 along with their composition has been confirmed using HR-TEM elemental mapping and EDAX analysis. To analyze the influence of $NiSe_2$ on TiO_2, different weight percentages of $NiSe_2$ loaded nanocomposite were prepared and measured the hydrogen evolution. Among all the nanocomposites, 25 wt.% $NiSe_2$ loaded nanocomposite exhibits maximum activity of 219.2 mmol/h/g_{cat} with solar to hydrogen conversion efficacy of 9%. To comprehend the effect of $NiSe_2$ as co-catalyst for the photocatalytic hydrogen evolution, the activity was compared with 1 wt.% Pt loaded TiO_2. Subsequently, the stability of optimized photocatalyst was also demonstrated for 5 cycles. After completion of 5 cycles, the physicochemical stability of the recovered photocatalyst have been examined using XRD and HR-TEM analysis. It was found that the prepared system retains excellent crystalline and structural stability. For better justification, the performance of prepared system is compared with the state of art photocatalysts. In addition, DFT calculations were performed to demonstrate the intrinsic role of $NiSe_2$ on TiO_2 nanoparticle in the overall water splitting. The remarkable photocatalytic activity and long-term stability makes the $NiSe_2/TiO_2$ nanocomposite as a promising photocatalyst in the field of overall water splitting.

2. Experimental section

2.1. Materials and reagents

The details of the chemicals used in this manuscript are given in the supporting information (SI).

2.2. Synthesis of $NiSe_2$ nanoparticles using supercritical fluid assisted method

$NiSe_2$ nanoparticles were synthesized by supercritical fluid process. In a typical process, 0.52 g of selenium powder and 2 mL of hydrazine hydrate were sonicated for 15 min followed by addition of 0.96 g of nickel nitrate hexahydrate under continuous sonication for 15 min. Then, the above solution was transferred into supercritical reactor of 30 mL volume and placed in pre-heated furnace at 400 °C for 30 min. The obtained product was washed with DI water followed by ethanol and then dried at 60 °C in vacuum oven.

2.3. Synthesis of TiO_2 nanoparticles

TiO_2 nanoparticles were synthesized via well-known sol-gel process from titanium (IV) isopropoxide. In this process, 5 mL of titanium isopropoxide was dissolved in 50 mL of ethyl alcohol, and followed by 20 mL of water has been added to the above solution under constant stirring for 15 h. Afterwards, the crude product was isolated, dried and then subjected to annealing for 2 h at 450 °C in box furnace.

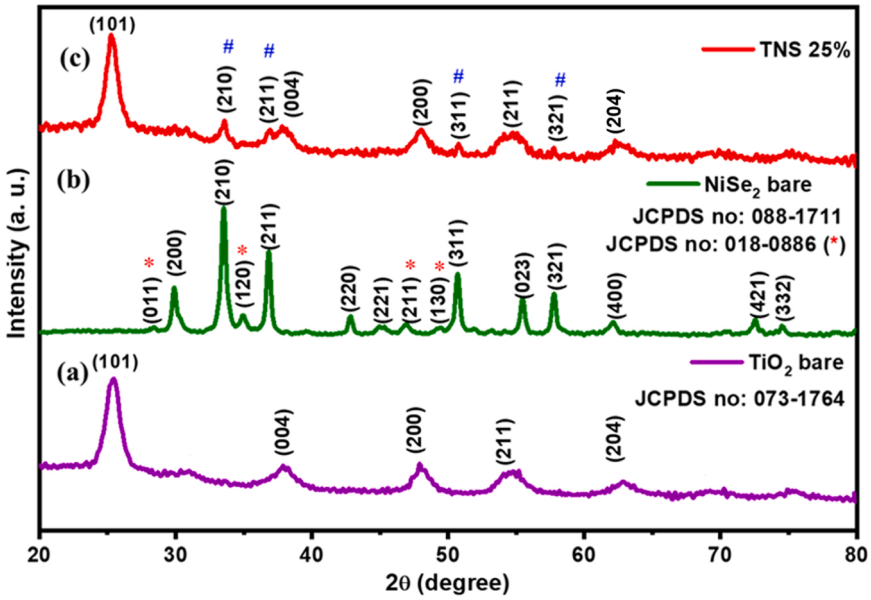

Fig. 1. XRD pattern of (a) TiO_2 nanoparticle (b) $NiSe_2$ nanoparticle (c) TNS 25% nanocomposite (# -represents diffracted patterns of $NiSe_2$).

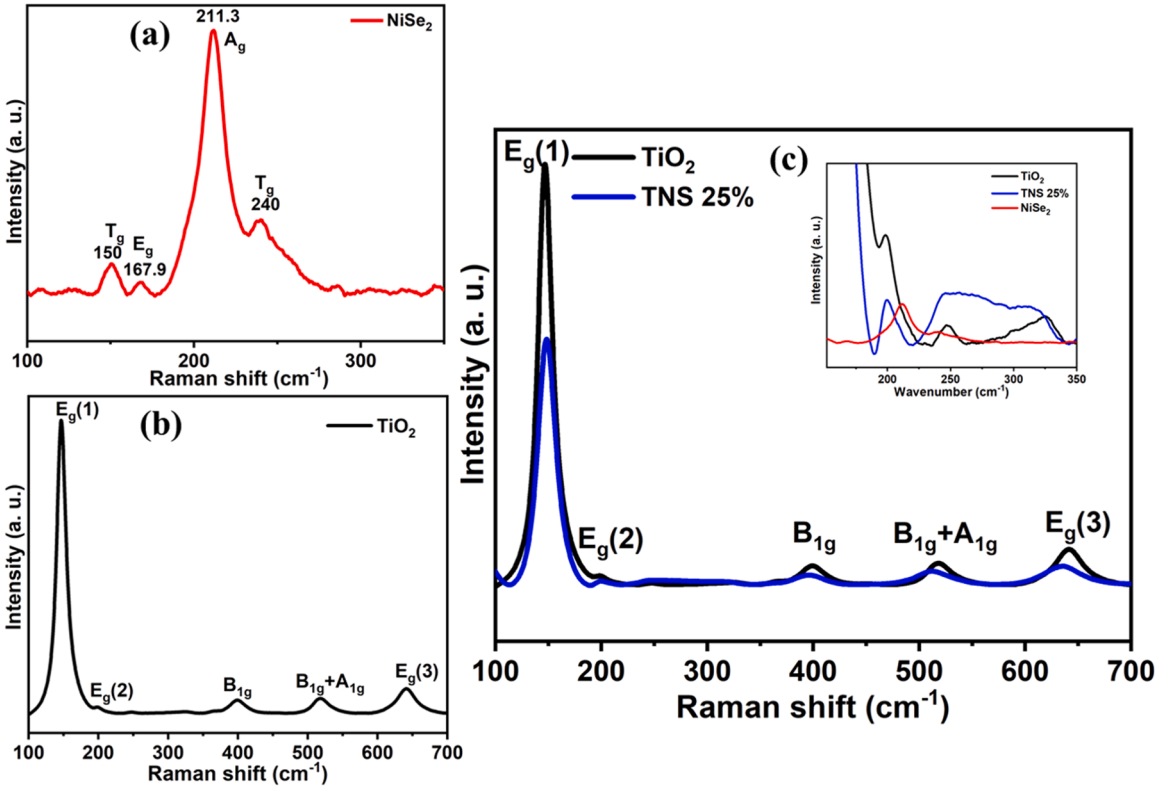

Fig. 2. Raman spectrum of (a) $NiSe_2$, (b) TiO_2, (c) TiO_2 and TNS 25% (inset: zoom in spectrum of pristine and optimized composite material).

2.4. Preparation of $NiSe_2/TiO_2$ nanocomposites

The preparation of $NiSe_2/TiO_2$ nanocomposites was carried out via wet impregnation method [48]. In this process, the prepared $NiSe_2$ and TiO_2 nanoparticles were dispersed using ethyl alcohol and water mixture (1:1 vol%), and maintained at 90 °C with continuous stirring up to get dried product. In order to scrutinize the photocatalytic activity of $NiSe_2/TiO_2$, different wt.% like 5%, 10%, 15%, 20%, 25%, 30%, 35% and 40% of $NiSe_2$ with respect to TiO_2 weight have been taken and denoted as TNS 5%, TNS 10%, TNS 15%, TNS 20%, TNS 25%, TNS 30%, TNS 35% and TNS 40%, respectively in the further discussions. The pictorial representation of $NiSe_2/TiO_2$ nanocomposite synthesis methodology is given in Scheme 1.

2.5. Characterization

The details of various analytical techniques employed to characterize the as prepared materials are given in supporting information (SI).

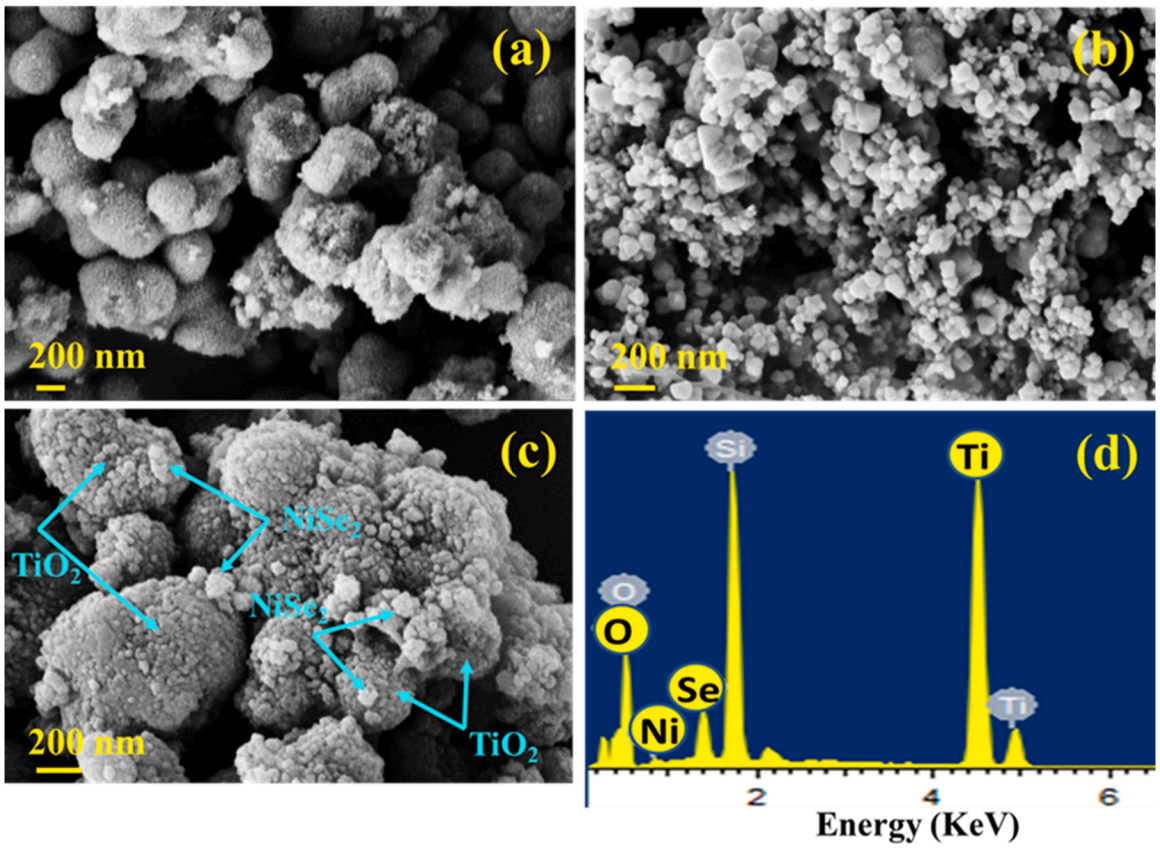

Fig. 3. FE-SEM images of (a) TiO_2, (b) $NiSe_2$, (c) TNS 25%, (d) EDX spectrum of TNS 25% nanocomposite.

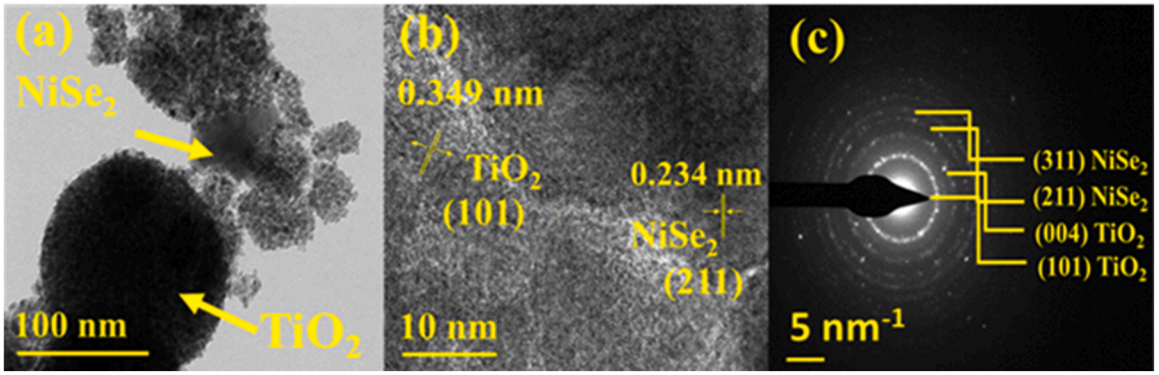

Fig. 4. (a-b) HR-TEM image of TNS 25%, (c) SAED pattern of TNS 25%.

2.6. Solar photocatalytic hydrogen evolution

Photocatalytic hydrogen generation experiments were performed using 450 W Xe-Hg lamp. To execute the experiments, 10 mg of as prepared nanocomposite was dispersed in a quartz reactor which contains an aqueous solution of glycerol (45 mL water + 5 mL glycerol) and subsequently the nitrogen purging was given to the sealed reactor for 30 min at ambient condition to evacuate the dissolved gases. Later, the whole setup was irradiated with 450 W Xe-Hg lamp, in accordance with constant rate of stirring. The course of illumination was executed for 4 h and the quantity of hydrogen produced has been measured for each 1 h interval by Shimadzu gas chromatograph (GC-2014) furnished with TCD detector. Moreover, the durability of optimized nanocomposite also examined for 5 cycles by kept the reactor in dark condition at the end of each cycle and purged with N_2 gas before moving to the succeeding cycle.

2.7. Computational methodology

To probe the feasibility of using $NiSe_2$ as a co-catalyst to enhance the rate of H_2 production over TiO_2 nanoparticle, density functional theory (DFT) studies were performed using Vienna Ab *initio* Simulation Package (VASP) with the projector augmented-wave (PAW) method [49,50]. Perdew-Burke-Ernzerhof (PBE) version of the generalized gradient approximations (GGA) [51] for the exchange-correlation functional were used to study the electronic and structural properties of the optimized structure. For structural optimization energy cut off value of plane wave basis was set to be 520 eV. All atoms in the system were fully relaxed with Hellman-Feynman force converging below to 0.03 eV/Å. To avoid interaction between original system and its periodic image, vacuum

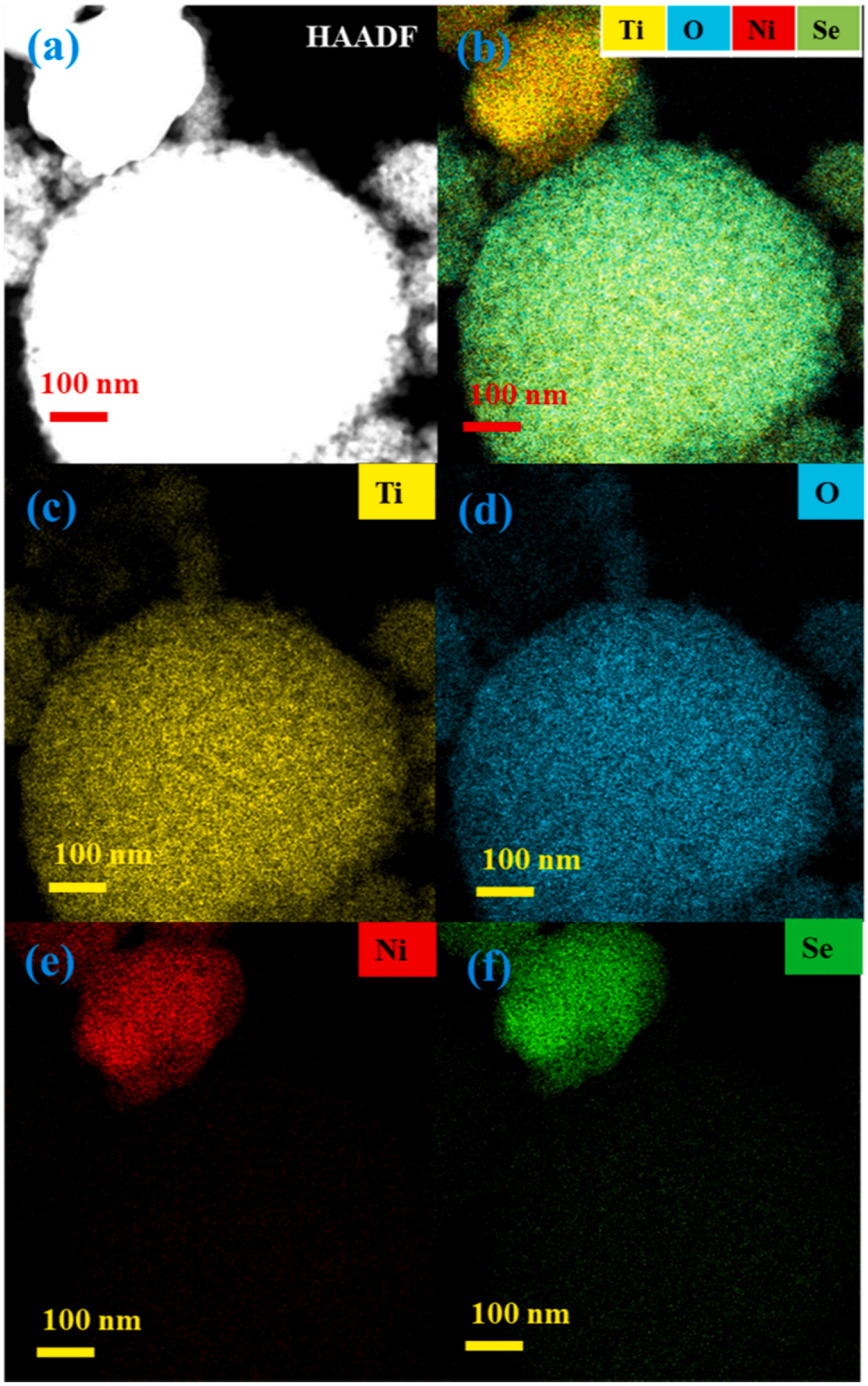

Fig. 5. HAADF image and elemental mapping of TNS 25% nanocomposite, (a) HAADF, (b) overall image (c) Ti, (d) O, (e) Ni and (f) Se elements distribution.

thickness placed in the z-direction was kept > 10 Å. Monkhrost-Pack [51] $3 \times 2 \times 1$ k-mesh was chosen for optimization of six layered (2×3) TiO_2 (101) surface slab and $NiSe_2/TiO_2$ structures. For treating Ni and Ti functionals, the effective U parameter of 4 eV [52] was considered.

3. Results and discussions

3.1. Structural characterisation

XRD pattern of as prepared samples are shown in Fig. 1. The diffraction pattern in Fig. 1(a) reflects successful formation of anatase TiO_2 tetragonal phase, which is in good agreement with the previously reported patterns and the JCPDS no: 073–1764. Fig. 1(b) shows the diffraction lines of $NiSe_2$, where two phases of $NiSe_2$ are observed in which the lines with (*) symbol represents orthorhombic phase and rest of lines were attributed to cubic phase. Fig. 1(c) explains XRD pattern of TNS 25% nanocomposite, where the lines with (#) represents (210), (211), (311) and (321) planes of cubic $NiSe_2$ and remaining lines were corresponding to TiO_2 nanoparticles. Here, it clearly displays the cubic phase of $NiSe_2$ is present with anatase TiO_2 thereby confirms successful formation of $NiSe_2/TiO_2$ nanocomposite.

Furthermore, to confirm the existence of $NiSe_2$ on TiO_2, the Raman spectrum of as prepared TiO_2, $NiSe_2$, TNS 25% were recorded and compared in Fig. 2. Raman spectrum of bare $NiSe_2$ exhibits (Fig. 2(a)) four characteristic peaks centered at 150(T_g), 167.9(E_g), 211.3(A_g), 240

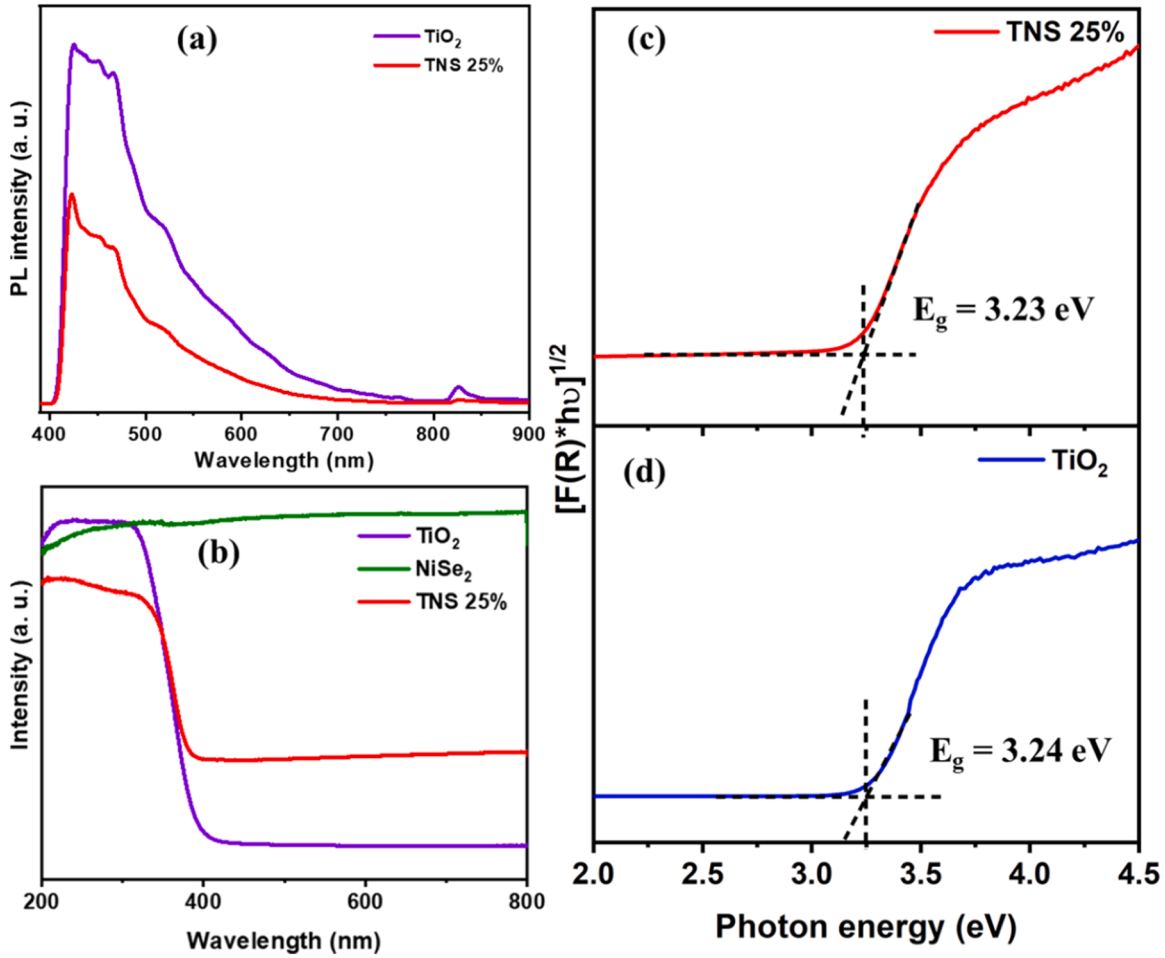

Fig. 6. (a) Photoluminescence spectrum of TiO_2 and TNS 25% nanocomposite, (b) absorption spectrum of TiO_2, $NiSe_2$ and TNS 25%, tauc plot of (c) TNS 25% nanocomposite and (d) TiO_2.

cm^{-1}(T_g) in which the peak at lower energy region (T_g and E_g) are due to vibrational modes of dumb-bell shaped Se_2 whereas higher energy regions (A_g and T_g) are corresponding to stretching mode of Se-Se pairs which are in good agreement with reported spectrum [53]. The Raman spectrum of bare anatase TiO_2 phase (Fig. 2(b)) predominantly exhibits six vibrational modes positioned at 146.6, 198.4, 641.4 (E_g), 399.6 (B_{1g}), and 518.2 cm^{-1} (A_{1g}+B_{1g}) which are also in good accordance with the reported spectrum [54]. And the spectrum of TNS 25% nanocomposite (Fig. 2(c)) shows broad spectral overlap between 220 and 340 cm^{-1} compared to the TiO_2 which is due to the interaction of TiO_2 and $NiSe_2$ also observed in the DFT investigation (Fig. 9(a)). To clearly see the spectral overlap, the zoom in spectrum is given in inset of Fig. 2 (c).

The surface morphology and particle size of synthesized samples are examined using FE-SEM and HR-TEM techniques, respectively. Fig. 3(a-b) show FE-SEM images of TiO_2 and $NiSe_2$ in which both materials possess the particle morphology. Furthermore, the morphology of TNS 25% nanocomposite is given in Fig. 3(c), which shows that the $NiSe_2$ nanoparticles are spread over the surface of TiO_2. This will enable the roughness to the surfaces of TiO_2 nanoparticles and it is speculated that, the enormous active sites are available at the surface of $NiSe_2$/TiO_2 nanocomposite. Fig. 3(d) displays FE-SEM EDAX spectrum of as prepared TNS 25% nanocomposite which implies the presence of $NiSe_2$ and TiO_2 in prepared nanocomposite. Furthermore, to confirm the local dispersion of $NiSe_2$ on TiO_2 nanoparticle, HR-TEM analysis was taken for TNS 25% nanocomposite. Fig. 4(a) shows HR-TEM image of TNS 25% nanocomposite which strongly indicates that, the $NiSe_2$ nanoparticles are uniformly dispersed over TiO_2. Moreover, the high magnification HR-TEM image (Fig. 4(b)) shows the lattice fringes of TNS 25% nanocomposite and the calculated *d* space values 0.34 nm and 0.23 nm are attributed to the (101) plane of TiO_2 and (211) plane of $NiSe_2$, and which are in good agreement with *d* space values obtained from XRD. The SAED pattern of TNS 25% nanocomposite displays many discrete rings, which are attributed to the polycrystalline nature of both TiO_2 and $NiSe_2$ (Fig. 4(c)). The diffraction rings indexed as (101) and (004) planes correspond to TiO_2 and the (211) and (311) planes correspond to $NiSe_2$ nanoparticles. Moreover, the formation of TNS nanocomposite was also confirmed by HAADF elemental mapping and depicted in Fig. 5. it is clear that $NiSe_2$ is in firm enough contact with TiO_2 for effective charge separation process which reduces the rate of charge recombination during photocatalytic hydrogen evolution.

In order to understand the charge recombination process, the photoluminescence (PL) properties of TiO_2 and TNS 25% nanocomposite were analyzed (Fig. 6(a)). The emission spectrum observed at 420 nm reveals that the pure TiO_2 has strong PL intensity compared to TNS 25% nanocomposite due to the higher recombination rate compared to $NiSe_2$/TiO_2 nanocomposite where the excited electron -hole pairs were separated efficiently by $NiSe_2$ co-catalyst. Consequently, the light harvesting property of nanocomposite was also studied by UV-Visible spectroscopy. The absorbance spectrum of TiO_2, $NiSe_2$, TNS 25% and the corresponding band gap energies are shown in Fig. 6(b) and (c and d), respectively. Here, bare $NiSe_2$ shows continuous absorption throughout the wavelength region (200–800 nm) which reflects its metallic character [39,52] besides the absorbance spectrum of TiO_2 and

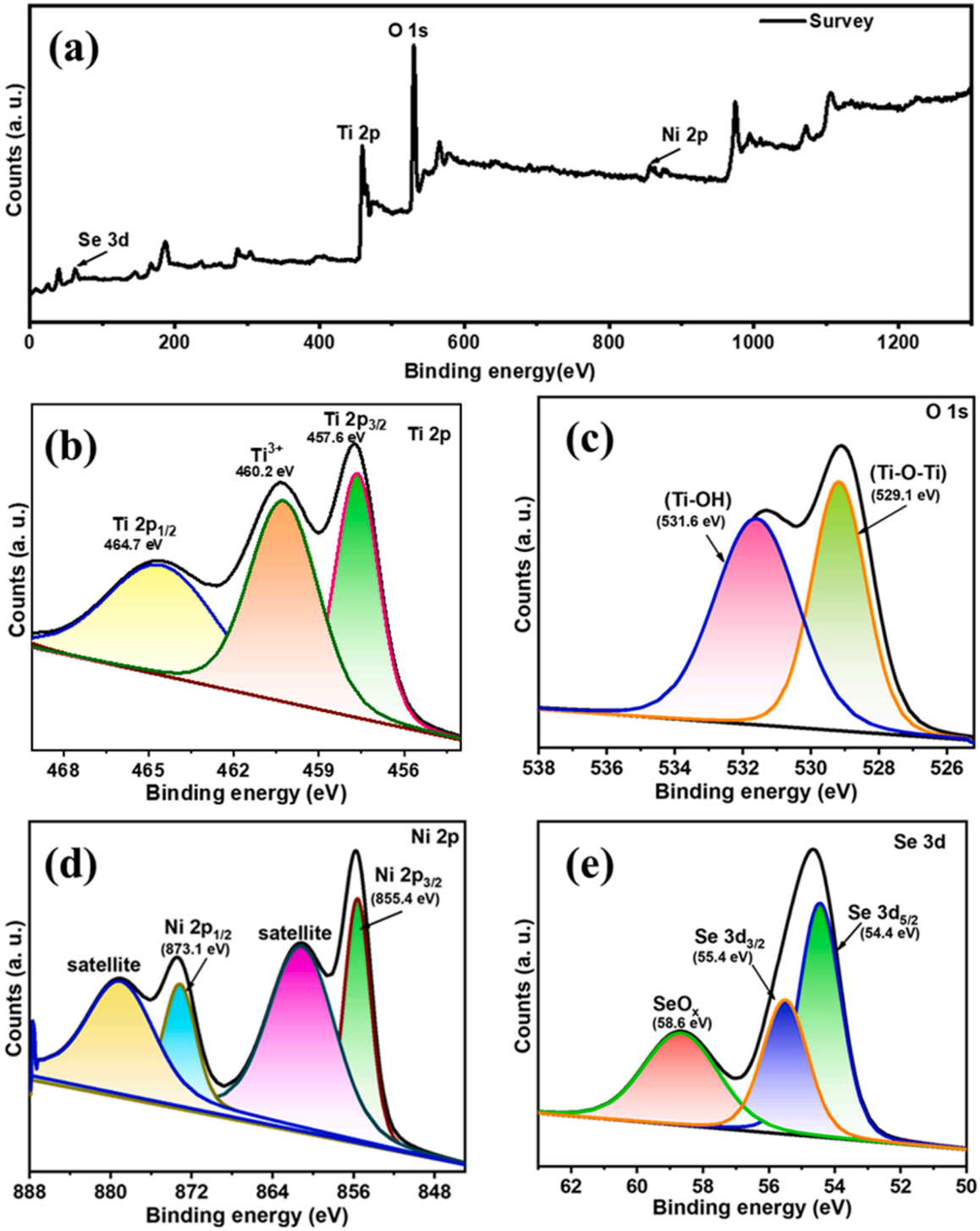

Fig. 7. (a) XPS survey spectrum of TNS 25% nanocomposite, (b) deconvoluted spectrum of Ti 2p, (c) O 1s, (d) Ni 2p, (e) Se 3d.

TNS 25% nanocomposite was not much changed. The band gap of TiO_2 and TNS 25% nanocomposite are almost same. It infers that $NiSe_2$ nanoparticles only covered on the surface of TiO_2 but not incorporated in to the lattice of TiO_2. Moreover, it also revealed that, the immobilized $NiSe_2$ helps electron tunnelling process but it does not significantly influence the optical properties of TiO_2.

To analyze the binding nature and the chemical states of the elements present in $NiSe_2/TiO_2$ nanocomposite, X-ray photoelectron spectrum is recorded (Fig. 7). Fig. 7(a) shows XPS survey spectrum of TNS 25% nanocomposite, which explains the presence of Ni, Se, Ti, and O elements in as-prepared nanocomposite. The deconvoluted spectrum of Ti^{4+} (Fig. 7(b)) shows peaks at 457.6 eV and 464.7 eV corresponds to Ti $2p_{3/2}$ and Ti $2p_{1/2}$. The additional peak at 460.2 eV represents Ti^{3+} ion, is due to oxygen vacancy in TiO_2 lattice which helps to narrow the band gap and reduces the rate of recombination of electron-hole pair [55]. The deconvoluted spectrum of O 1s shown in Fig. 7(c) displays a pair of peaks at 529.1 eV and 531.6 eV attributed to Ti-O-Ti (lattice oxygen) and Ti-O-H (absorbed on the surface) [56]. Fig. 7(d) explains the deconvoluted spectrum of Ni 2p in which the doublet at 855.4 eV and 873.1 eV represents Ni $2p_{3/2}$ and Ni $2p_{1/2}$ is due to spin orbit coupling. The two additional shoulder peaks found at 861 eV and 879 eV are satellite peaks of Ni 2p [57]. Fig. 7(e) depicts the

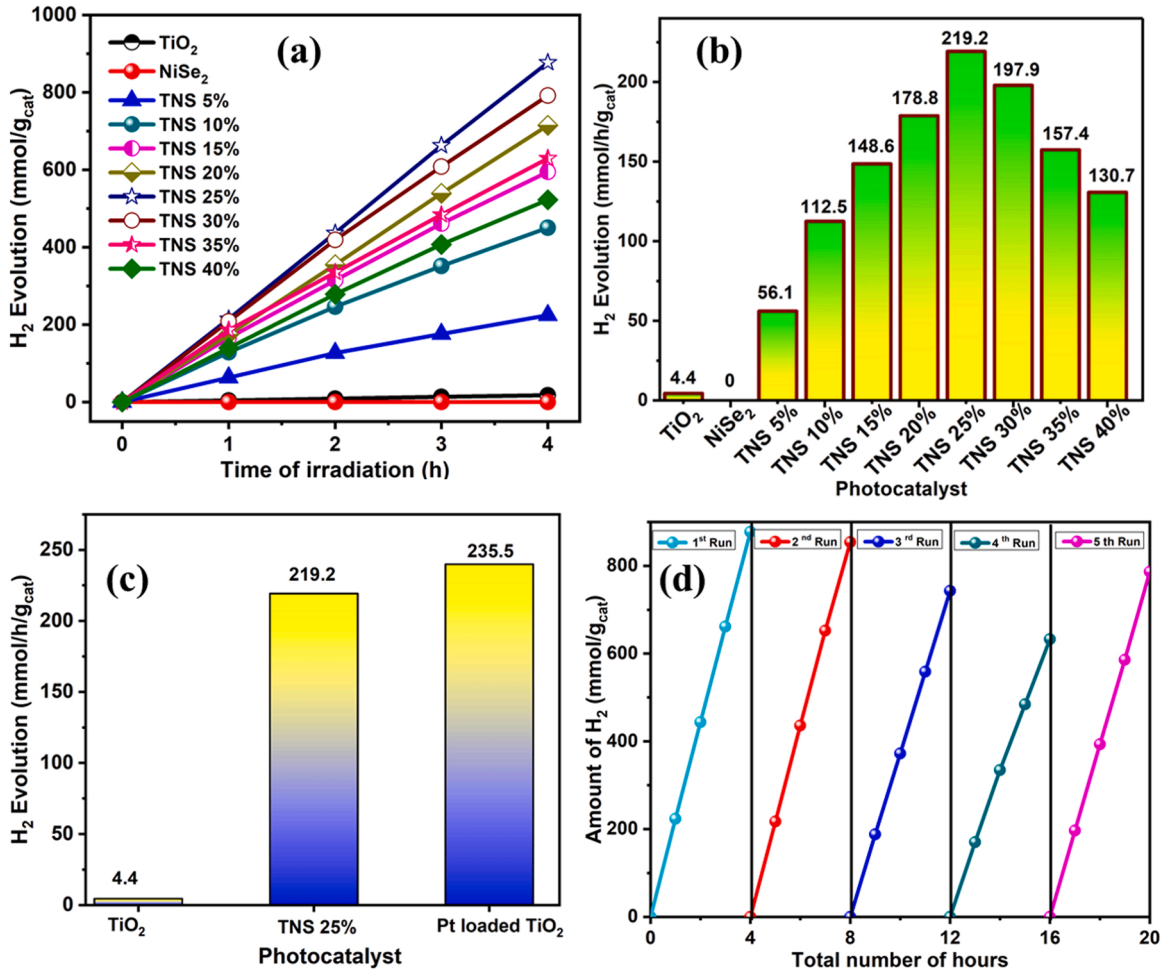

Fig. 8. The photocatalytic activity profile of TiO_2, $NiSe_2$ and various TNS nanocomposites (a) hydrogen production with respect to time, (b) average rate of hydrogen production, (c) comparison profile for average rate of hydrogen production of TiO_2, TNS 25%, 1 wt.% Pt loaded TiO_2, (d) photostability study of TNS 25% nanocomposite.

deconvoluted spectrum of Se 3d whereas the peaks at 54.4 eV and 55.4 eV correspond to $3d_{5/2}$ and $3d_{3/2}$, respectively. The additional peak at 58.6 eV is due to high valent oxide of selenium [57].

3.2. *Photocatalytic activity of $NiSe_2/TiO_2$ nanocomposite*

TiO_2 is a well-known stable photocatalyst with suitable band edge positions for photocatalytic hydrogen production, even though its photocatalytic performance is limited by fast charge recombination. Here, $NiSe_2$ loaded TiO_2 is used for photocatalytic hydrogen generation from aqueous glycerol solution. The photocatalytic performance of prepared TNS nanocomposites has been studied by irradiating 10 mg of prepared photocatalyst dispersed in 50 mL of aqueous glycerol solution (10 vol%) with 450 W Xe-Hg lamp. Fig. 8(a) displays the hydrogen production rate comparison profile of TiO_2, $NiSe_2$, and prepared TNS nanocomposites with respect to time. From which it is clear that, TiO_2 produces very less amount of hydrogen because of wide band gap and fast recombination of photogenerated charge carries while the bare $NiSe_2$ doesn't produce any hydrogen evolution due to its metallic nature. Interestingly, all other $NiSe_2$ loaded TiO_2 nanocomposite exhibits the improved amount of hydrogen compare to TiO_2 which in turn explains a greater number of electrons employed for the reduction reaction thereby the recombination of photogenerated charged spices decreased significantly. However, the hydrogen production rate increased with $NiSe_2$ loading up to 25 wt. % and further increment of $NiSe_2$ co-catalyst loading leads to decrease in the rate of hydrogen production. This is attributed to agglomeration of $NiSe_2$ particles over TiO_2 surface which hinders the light absorption ability of TiO_2 nanoparticles. Fig. 8(b) displays the average hydrogen production rate of TiO_2, $NiSe_2$, and TNS nanocomposite as bar diagram. This graph evidently explains that, the TiO_2 nanoparticles produces very poor hydrogen evolution rate of 4.4 mmol/h/g_{cat} and all TNS nanocomposites delivers significantly high rate of hydrogen production. Among them 25 wt.% $NiSe_2$ loaded TiO_2 exhibits a huge amount of hydrogen production rate of 219.2 mmol/h/g_{cat}. Further increment of $NiSe_2$ on TiO_2 leads to decrease in activity due to agglomeration of $NiSe_2$ as discussed earlier. For well justification, the obtained rate of hydrogen production for 25 wt.% $NiSe_2$ loaded TiO_2 system is compared with 1 wt.% Pt loaded TiO_2 Fig. 8(c)). it is clear from the results that the Pt loaded TiO_2 shows the hydrogen production rate of 235.5 mmol/h/g_{cat} which is slightly higher than that of optimized TNS 25% nanocomposite (219.2 mmol/h/g_{cat}). Thus, the hydrogen production rate of prepared TNS 25% nanocomposite is much closer to that of Pt loaded TiO_2. It concludes that $NiSe_2$ is one of the best alternative co-catalysts for noble Pt metal in photocatalytic hydrogen production because of its conductive nature.

However, photostability of the designed system is one of the major issues in the photocatalytic water splitting. Hence, to reveal the photostability of optimized $TiO_2/NiSe_2$ nanocomposite, a time course of gas evolution has been studied for 5 days of 4 h in each day as shown in Fig. 8(d). At the end of each day experiment, the quartz reactor was kept in dark condition and purged with nitrogen gas before moving to the next day experiment. From Fig. 8(d), it could be clearly understood that,

Table 1
The comparison of rate of hydrogen production by optimized $NiSe_2/TiO_2$ nanocomposite with other reports.

S. No	Photocatalyst	Light Source	Sacrificial reagent	H_2 evolution (mmol/h/g_{cat})	Ref
1.	$CdS/NiSe_2$	300 W Xe lamp (AM 1.5 filter)	Lactic acid	61.52	[45]
2.	$NiSe_2/ZnIn_2S_4$	300 W Xe lamp $\lambda > 420$ nm	TEOA	1.48	[46]
3.	$NiSe_2/Mn_{0.05}Cd_{0.95}S$	5 W LED white light	Na_2S/Na_2SO_3	14.3	[47]
4.	$NiSe_2$/MIL-53 (Fe)	300 W Xe lamp ($\lambda > 420$ nm)	Lactic acid	10.3	[44]
5.	Ag/TiO_2	UV light ($\lambda = 254$ nm, 4.40 mW/cm^2)	Na_2S/Na_2SO_3	23.5	[65]
6.	Cu-TiO_2	300 W Xe lamp ($\lambda > 420$ nm)	TEOA	5.9	[66]
7.	PtO@Ti_3C_2/TiO_2	PLS-SXE-300 C lamp (13.31 mW/cm^2)	Methanol	2.54	[67]
8.	Ti_3C_2Tx/TiO_2	200 W Hg lamp (cut off at 285 −325 nm)	Methanol	2.65	[68]
9.	ZnO/TiO_2-Au	UV Pen-Ray Lamp (4.4 mW/cm^2)	Methanol	9.13	[69]
10.	Cu_2O/TiO_2	300 W Xe lamp	Methanol	32.6	[70]
11.	0D Co_3O_4/1D TiO_2	UV-Visible light	Methanol	3.46	[71]
12.	Co_9S_8/CdS	450 nm LED lamp (100 mW/cm^2)	Benzyl alcohol	61.9	[72]
13.	$Fe_4Ni_5S_8$ @$ZnIn_2S_4$	300 W Xe lamp (420 nm cut-off filter)	Benzyl alcohol	10.4	[73]
14.	**$NiSe_2/TiO_2$**	450 W **Xe-Hg lamp**	**Glycerol**	**219.2**	**Present work**

Table 2
STH conversion efficiency for TiO_2, Pt loaded TiO_2, and all prepared TNS nanocomposite.

S. No:	Name of the photocatalyst	Rate of H_2 evolution (mmol/h/g_{cat})	STH (%)
1.	TiO_2	4.4	0.18
2.	TNS 5%	56.1	2.3
3.	TNS 10%	112.5	4.6
4.	TNS 15%	148.6	6.1
5.	TNS 20%	178.8	7.4
6.	**TNS 25%**	**219.2**	**9**
7.	TNS 30%	197.9	8.2
8.	TNS 35%	157.4	6.5
9.	TNS 40%	130.7	5.4
10.	Pt loaded TiO_2	235.5	9.7

the photocatalytic activity of TNS 25% nanocomposite for first two days experiments is nearly similar, whereas on 3rd and 4th day experiments a slightly linear downturn in activity is noticed. Here, it is speculated from our earlier experiences that, the observed nature is due to decrease in concentration of glycerol. To disclose this supposition, 5 mL of glycerol is added to the test solution before moving to the 5th day experiment and an increased rate of activity as equivalent to that of first two days has been observed with the retention of 89% activity. From this it is clearly witnessed that, the concentration of glycerol also plays a significant role for successful photocatalytic hydrogen evolution. Furthermore, the physicochemical stability of the recovered photocatalyst (after 5th cycle) is also investigated using XRD, HR-TEM and TEM-EDAX analysis as given in supporting information Fig. S1, S2 and S3, respectively. From Fig. S1, it observed that the XRD pattern of TNS 25% nanocomposite before and after activity is almost similar. And Fig. S2 disclosed that contact between TiO_2 and $NiSe_2$ in the TNS 25% nanocomposite fair enough to execute the photocatalytic performance for prolonged reaction. Moreover, the atomic composition of $NiSe_2/TiO_2$ after activity is calculated using TEM-EDAX and compared with that of fresh photocatalyst (Fig. S3). From the results it is manifestly observed that, the prepared system has firm enough stability as composite with appropriate composition.

Finally, the photocatalytic performance of prepared system ($NiSe_2/TiO_2$) has been compared with few recently reported systems (Table 1). From the existed results, it is clearly evidenced that, the rate of activity obtained for the present system ($TiO_2/NiSe_2$) is much greater than that of other reported systems and is almost closer to the performance of Pt loaded TiO_2 system. However, from these analyses it is verified that, the $NiSe_2$ prepared in this work is an effective co-catalyst to enhance the photocatalytic hydrogen evolution in grand manner.

3.3. Solar to hydrogen conversion efficiency calculation

Solar to hydrogen conversion efficiency (STH) was calculated for all the bare and nanocomposites photocatalysts using the following formula [58].

$$\text{Solar } to\ H_2 \text{ conversion } efficiency(\%) = \frac{\text{Output energy as } hydrogen}{\text{The energy of incident } light}$$

$$\text{STH} = \frac{\text{rH}_2 \quad \times \Delta G}{\text{P}_{light} \times \text{S}}$$

$$\text{STH} = \frac{\text{rH}_2 \quad (\text{mmol}sec^{-1}) \quad \times \Delta G \quad (237,000 \quad J \quad mol^{-1})}{\text{P}_{light} \quad (\text{mW}cm^{-2}) \times \text{S}(cm^2)}$$

where, rH_2 is the rate of hydrogen production (mmol/s), ΔG is the gain in Gibbs free energy (J/mol).), S is the area of the reactor (cm^2) and P_{light} is energy flux of the incident light (mW/cm^2). The calculated solar to hydrogen conversion efficiency values are depicted in the Table 2.

3.4. Photoelectrochemical properties of $NiSe_2/TiO_2$ nanocomposite

To understand the photogenerated charge transfer process in the $NiSe_2/TiO_2$ nanocomposite, the photoelectrochemical studies were performed using 1 M KOH electrolyte under the illumination of AM 1.5G (100 mW/cm^2). Photocurrent is increased upon illumination and decreased rapidly to zero when the light is switched off. Fig. 9(a) shows photocurrent-time response of pure TiO_2 and TNS 25%. It can be seen that, pure TiO_2 shows relatively low photo-current density, explaining low charge transfer rate for surface reaction, which eventually may increase the recombination rate of charge carriers. Whereas, the $NiSe_2$ loaded TiO_2 exhibits high photocurrent density compared to bare TiO_2 infers a greater number of photoexcited electrons existed in the $NiSe_2/TiO_2$ composite under illumination. Moreover, the observed photocurrent spike in the initial stage of irradiation implies charge separation is occurs in the composite [59]. From these factors, it is clear that, the charge separation and facile transportation happened due to the presence of $NiSe_2$ over the TiO_2 and it obviously reduces the rate of surface charge recombination. These results are in good agreement with the experimental observations of photocatalytic H_2 production over TiO_2 and TNS 25% nanocomposite.

Furthermore, to validate the above inference, the electrochemical impedance spectroscopy is also analyzed. Fig. 9(b) shows the Nyquist plot of TiO_2 and TNS 25% nanocomposite under illuminated condition. According to the previous literature [59], the interfacial charge transfer resistance of the material is measured by diameter of semi-circle in the Nyquist plot. It can be clearly seen that, the R_{ct} value of TNS 25% nanocomposite is significantly low compared to bare TiO_2, suggesting

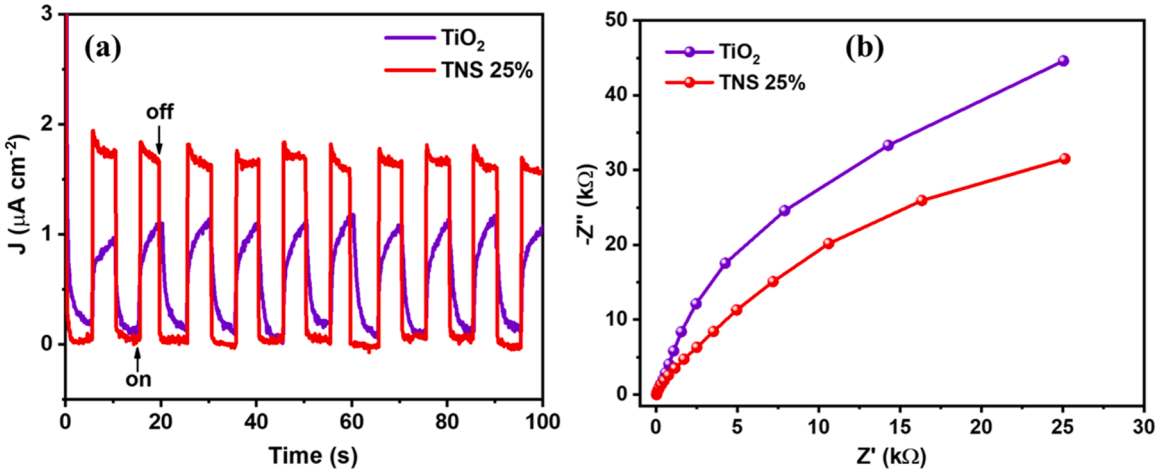

Fig. 9. (a) Transient photocurrent-time curves of TiO_2 and TNS 25% nanocomposite (b) Nyquist plot of TiO_2 and TNS 25%.

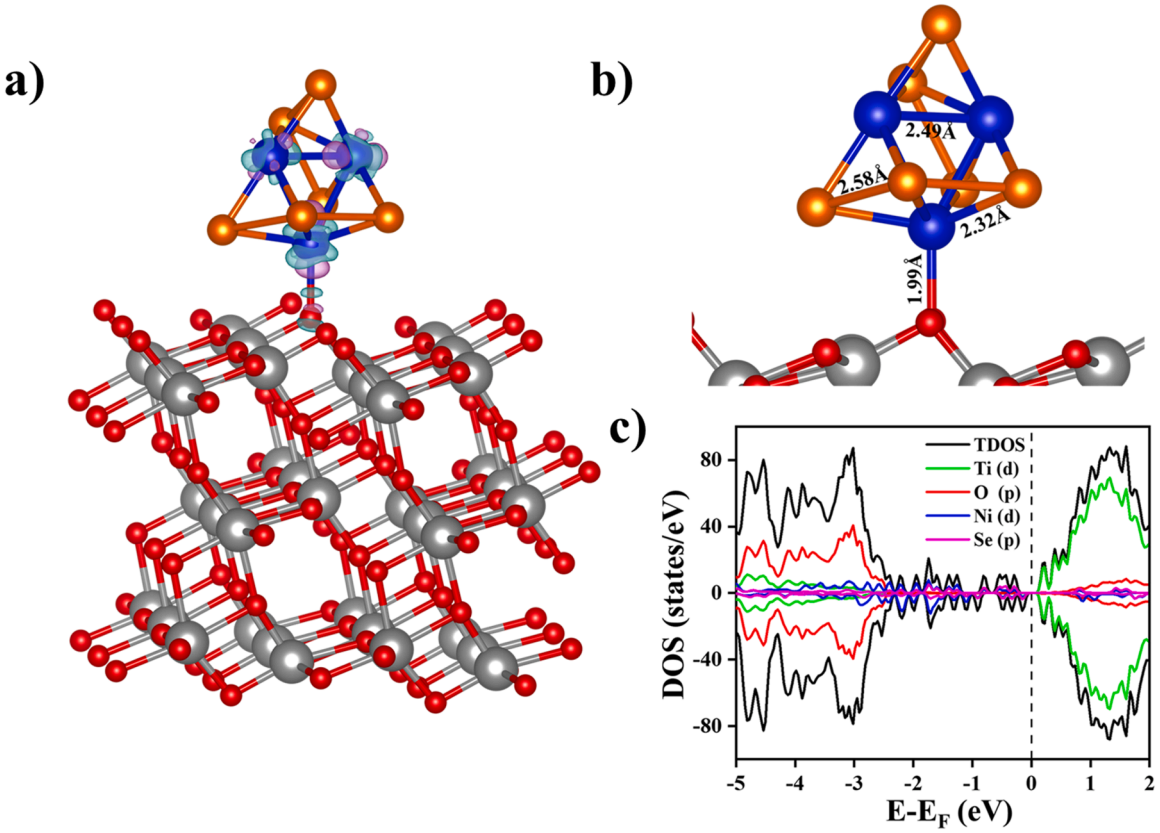

Fig. 10. (a) The charge density differences of TNS nanocomposites are shown. Grey, red, blue, yellow balls represent Ti, O, Ni, and Se atoms, respectively. The charge density is represented by excess charge light blue (depletion charge-pink color) iso-surface (value is 0.01 $e^-/Å^3$). b) Bond length of the adsorbed cluster c) DOS plot of TNS nanocomposite.

that interfacial charge transfer is highly facilitated in the composite due to the presence of highly conductive $NiSe_2$ nanoparticles over the surface of TiO_2. This rapid charge transfer can promote the efficient separation of electron-hole pair which helps to decrease the charge recombination in the composite. Thus, it is proved that the loading of $NiSe_2$ over TiO_2 surface could effectively insist the rapid transfer of photogenerated electrons which promotes the photoexcited electron-hole pair separation, thereby enhancing the better rate of photocatalytic hydrogen production.

3.5. *DFT study: influence of $NiSe_2$ on photocatalytic property of TiO_2*

In order to prove the experimental findings, stable Ni_3Se_6 cluster which was deduced by performing various possible isomers was considered for depositing onto TiO_2 anatase (101) surface. It was constructed by (2 × 3) supercell and then, optimized using first principles DFT calculations as described in above section. The calculated lattice parameters of surface slab (a(Å), b(Å), γ) is to be (5.62, 3.73, 110.3°), which is quite consistent with previous studies[60,61]. Further, Ni_3Se_6 cluster is found to be magnetic with the spin moment of ~2 μ_B. It is also

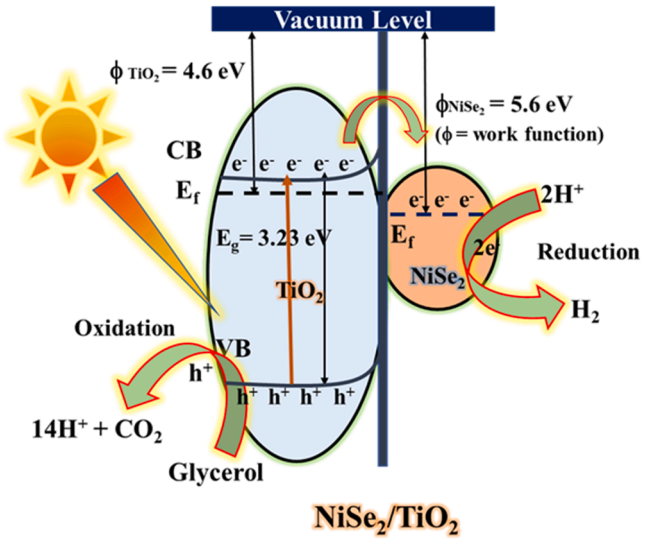

Fig. 11. Plausible mechanism of photocatalytic hydrogen evolution over $NiSe_2/TiO_2$ nanocomposite.

observed that Ni-Se, Ni-Ni and Se-Se bond distances are 2.32, 2.49, and 2.58 Å, respectively as shown in Fig. 10(b), indicating the presence of Se_2 dimer as observed by our experiment. The Ni_3Se_6 cluster is deposited onto TiO_2 (101) surface slab to mimicking TNS nanocomposite. The adsorption energy (E_{ads}) is calculated to be − 0.6 eV and it was deduced from $E_{ads} = E_{total} - [E_{surf} + E_{cluster}]$. Here, E_{total}, E_{surf} and $E_{cluster}$ are the total energies of TNS, TiO_2 surface slab and $NiSe_2$ cluster, respectively. This negative value indicates formation of TNS nanocomposite.

To understand the interaction between the cluster and TiO_2 surface, the charge density difference ($\Delta\rho$) is calculated as $\Delta\rho = \rho_{TNS} - \rho_{surf} - \rho_{cluster}$, where ρ_{TNS}, ρ_{surf}, and $\rho_{cluster}$ are charge densities of TNS composite, TiO_2 surface slab and $NiSe_2$ cluster, respectively. The excess and depletion of charge densities of system is plotted as shown in Fig. 10(a). It infers that the structural stability of TNS composite is attributed by forming sigma bond between cluster and TiO_2 surface.

The density of states (DOS) of TNS is also reported in Fig. 10(c). In the pristine TiO_2 surface slab, top of the valence band (VB) is mainly contributed by the O-2p orbitals, while the bottom of the conduction band (CB) is comprised by Ti-3d states. The VB and CB are separated by the energy gap of ~2.5 eV. On deposition of cluster on the TiO_2 surface, the part of Ni-3d and Se-4p states are occupied in the band gap region of TiO_2. It is also noticed in DOS that these states are well hybridized between Ni-3d and Se-4p states and they are responsible electrical conductivity of $NiSe_2$ nanoparticles. Overall, the photo-excited electron in the CB of TiO_2 is migrated to these hybridized states where it will be utilized for hydrogen production. On the other hand, the holes presented in the VB of TiO_2 are used for oxidation. Since, the oxidation and reduction reactions are occurred respectively, on TiO_2 and $NiSe_2$ surfaces, the recombination of the charge carriers is expected to be avoided.

3.6. Plausible mechanism over $NiSe_2/TiO_2$ nanocomposite for photocatalytic hydrogen production

On the basis of results obtained from both experimental and theoretical studies, feasible mechanism for $NiSe_2/TiO_2$ nanocomposite under the light illumination is proposed (Fig. 11). When the $NiSe_2/TiO_2$ nanocomposite was illuminated with light, TiO_2 nanoparticles absorb the light energy thereby electron gets excited from valence band to conduction band leaving the holes in the valence band (Eq. (1)). The excited electrons are trapped out by $NiSe_2$ due its highly conductive nature and favorable energy level. Since, the work function of $NiSe_2$ (5.6 eV) [62] is greater than that of TiO_2 (4.6 eV) [63], effective charge transfer from the conduction band of TiO_2 to $NiSe_2$ facilitated that leads to develop built in electric filed across the $NiSe_2$-TiO_2 junction, which causes upward bending of energy bands. The built-in electric filed strongly prevents the migration of electrons from $NiSe_2$ to TiO_2, thereby the separation electron-hole pair is highly encouraged. The holes at the valance band of TiO_2 react with water to produce hydroxy radical and H^+ ions (Eq. (2)). Then, the produced hydroxyl radical reacts with glycerol to form the intermediates like aldehyde and acid, finally, due to decarboxylation CO_2 is produced as by product (Eq. (3)) [64]. The H^+ ions get reduced to H_2 by the trapped electrons in $NiSe_2$ over the surface of TiO_2. Owing to highly conductive nature of $NiSe_2$, the electron transportation to the surface reaction is highly enhanced which suppress the charge recombination in TiO_2 and enhances the rate of hydrogen production.

$$TiO_2 \xrightarrow{hv} h^+ + e^- \quad (1)$$

At valance band of TiO_2

$$3H_2O + 3h^+ \rightarrow 3H^+ + \quad 3OH^* \quad (2)$$

The formed hydroxyl radical reacts with adsorbed glycerol and form the reaction intermediates like aldehyde, acid and finally CO_2 as by product.

$$C_3H_8O_3 + 3OH^* + 11h^+ \rightarrow Intermediates \quad (C_3H_6O_3, C_2H_4O_3, C_2H_2O_3, C_2H_4O_3, etc) \rightarrow 3CO_2 + 11H^+ \quad (3)$$

Reaction at $NiSe_2$ surface,

$$14H^+ + \quad 14e^- \rightarrow 7H_2(g)$$

4. Conclusion

$NiSe_2$ nanoparticles and $NiSe_2/TiO_2$ nanocomposite were successfully synthesized using short time reaction based supercritical fluid assisted method and wet impregnation process, respectively. The prepared materials thoroughly examined using various characterization techniques especially XRD, Raman, HR-TEM, and XPS analysis. The photocatalytic activity of TiO_2 was greatly enhanced in presence of $NiSe_2$. The optimized photocatalyst TNS 25% showed a maximum photocatalytic activity of 219.2 mmol/h/g_{cat} under continuous irradiation with excellent stability of 89% after 5 cycles. Furthermore, with the help of DFT study, the role of $NiSe_2$ on TiO_2 in $NiSe_2/TiO_2$ nanocomposite for overall water splitting was established. The results obtained from theoretical calculations confirms that, the enhanced photocatalytic activity of TiO_2 is due to metallic states of $NiSe_2$ that facilitates the facile electron transfer thereby effective e^-/h^+ pair separation and more active sites availing for hydrogen evolution. This work proven that $NiSe_2$ could be an effective co-catalyst to elevate the photocatalytic activity of semiconductor photocatalyst and $NiSe_2/TiO_2$ nanocomposite could be a potential and practicable candidate for photocatalytic water splitting. This work stimulates and opens a new avenue for researchers to explore various other transition metal selenides as co-catalysts for photocatalytic water splitting.

CRediT authorship contribution statement

S. Jayachitra: Methodology, Investigation, Conceptualization, Data curation, Validation, DFT studies, Writing – original draft. **D. Mahendiran:** DFT studies and validation, Data curation, Writing – original draft. **P. Ravi:** Formal analysis, Investigation, Data curation, Validation, Writing – original draft. **P. Murugan:** Supervision, Writing – review & editing. **M. Sathish:** Supervision, Writing – review & editing.

Declaration of Competing Interest

The authors declare that they have no known competing financial interests or personal relationships that could have appeared to influence the work reported in this paper.

Acknowledgements

S. J and D. M is thankful for the financial support (UGC-Ref.No.: 359/ (CSIR-UGC NET JUNE 2017) and 1393/ (CSIR-UGC NET JUNE 2018)) by the Council of Scientific and Industrial Research (CSIR-UGC), New Delhi, for the award of Senior Research Fellowship (SRF). The authors thanks to the central instrumentation and high-performance computing facilities of CSIR-CECRI, Karaikudi.

CSIR-CECRI Manuscript communication number: CECRI/PESVC/ Pubs./2021–148.

Appendix A. Supporting information

Supplementary data associated with this article can be found in the online version at doi:10.1016/j.apcatb.2022.121159.

References

[1] K.C. Christoforidis, P. Fornasiero, Photocatalytic hydrogen production: a rift into the future energy supply, ChemCatChem 9 (2017) 1523–1544.
[2] C. Acar, I. Dincer, G.F. Naterer, Review of photocatalytic water-splitting methods for sustainable hydrogen production, Int. J. Energy Res. 40 (2016) 1449–1473.
[3] C.H. Liao, C.W. Huang, J.C.S. Wu, Hydrogen production from semiconductor-based photocatalysis via water splitting, Catalysts 2 (2012) 490–516.
[4] H. Ahmad, S.K. Kamarudin, L.J. Minggu, M. Kassim, Hydrogen from photocatalytic water splitting process: a review, Renew. Sustain. Energy Rev. 43 (2015) 599–610.
[5] N.L. De Silva, A.C.A. Jayasundera, A. Folger, O. Kasian, S. Zhang, C.F. Yan, C. Scheu, J. Bandara, Superior solar-to-hydrogen energy conversion efficiency by visible light-driven hydrogen production via highly reduced Ti^{2+}/Ti^{3+} states in a blue titanium dioxide photocatalyst, Catal. Sci. Technol. 8 (2018) 4657–4664.
[6] H. Wang, W. Chen, J. Zhang, C. Huang, L. Mao, Nickel nanoparticles modified CdS - A potential photocatalyst for hydrogen production through water splitting under visible light irradiation, Int. J. Hydrogen Energy 40 (2015) 340–345.
[7] G.J. Lee, S. Anandan, S.J. Masten, J.J. Wu, Photocatalytic hydrogen evolution from water splitting using Cu doped ZnS microspheres under visible light irradiation, Renew. Energy 89 (2016) 18–26.
[8] N. Wang, X. Li, Facile synthesis of CoO nanorod/C_3N_4 heterostructure photocatalyst for an enhanced pure water splitting activity, Inorg. Chem. Commun. 92 (2018) 14–17.
[9] H. Wang, W. Zhu, B. Chong, K. Qin, Improvement of photocatalytic hydrogen generation from CdSe/CdS/TiO_2 nanotube-array coaxial heterogeneous structure, Int. J. Hydrogen Energy 39 (2014) 90–99.
[10] J. Liu, Q. Jia, J. Long, X. Wang, Z. Gao, Q. Gu, Amorphous NiO as co-catalyst for enhanced visible-light-driven hydrogen generation over g-C_3N_4 photocatalyst, Appl. Catal. B Environ. 222 (2018) 35–43.
[11] Y. Lu, Y. Li, Y. Wang, J. Zhang, Two-photon induced NIR active core-shell structured WO_3/CdS for enhanced solar light photocatalytic performance, Appl. Catal. B Environ. 272 (2020), 118979.
[12] K. Villa, J.R. Galán-Mascarós, N. López, E. Palomares, Photocatalytic water splitting: advantages and challenges, Sustain. Energy Fuels 5 (2021) 4560–4569.
[13] L. Lin, T. Hisatomi, S. Chen, T. Takata, K. Domen, Visible-light-driven photocatalytic water splitting: recent progress and challenges, Trends Chem. 2 (2020) 813–824.
[14] K. Maeda, K. Domen, Photocatalytic water splitting: recent progress and future challenges, J. Phys. Chem. Lett. 1 (2010) 2655–2661.
[15] M.S. Nasir, G. Yang, I. Ayub, S. Wang, W. Yan, Tin diselinide a stable co-catalyst coupled with branched TiO_2 fiber and g-C_3N_4 quantum dots for photocatalytic hydrogen evolution, Appl. Catal. B Environ. 270 (2020), 118900.
[16] J. Liu, J. Ke, Y. Li, B. Liu, L. Wang, H. Xiao, S. Wang, Co_3O_4 quantum dots/TiO_2 nanobelt hybrids for highly efficient photocatalytic overall water splitting, Appl. Catal. B Environ. 236 (2018) 396–403.
[17] M. Ismael, A review and recent advances in solar-to-hydrogen energy conversion based on photocatalytic water splitting over doped-TiO_2 nanoparticles, Sol. Energy 211 (2020) 522–546.
[18] P. Ravi, V. Navakoteswara Rao, M.V. Shankar, M. Sathish, CuO@NiO core-shell nanoparticles decorated anatase TiO_2 nanospheres for enhanced photocatalytic hydrogen production, Int. J. Hydrogen Energy 45 (2020) 7517–7529.
[19] S. Jayachitra, P. Ravi, P. Murugan, M. Sathish, Supercritically exfoliated Bi_2Se_3 nanosheets for enhanced photocatalytic hydrogen production by topological surface states over TiO_2, J. Colloid Interface Sci. 605 (2022) 871–880.
[20] N. Fajrina, M. Tahir, A critical review in strategies to improve photocatalytic water splitting towards hydrogen production, Int. J. Hydrogen Energy 44 (2019) 540–577.
[21] Y. Li, S.C.E. Tsang, Recent progress and strategies for enhancing photocatalytic water splitting, Mater. Today Sustain. 9 (2020), 100032.
[22] K. Afroz, M. Moniruddin, N. Bakranov, S. Kudaibergenov, N. Nuraje, A heterojunction strategy to improve the visible light sensitive water splitting performance of photocatalytic materials, J. Mater. Chem. A 6 (2018) 21696–21718.
[23] A. Kudo, H. Kato, I. Tsuji, Strategies for the development of visible-light-driven photocatalysts for water splitting, Chem. Lett. 33 (2004) 1534–1539.
[24] D. Kim, K. Yong, Boron doping induced charge transfer switching of a C_3N_4/ZnO photocatalyst from Z-scheme to type II to enhance photocatalytic hydrogen production, Appl. Catal. B Environ. 282 (2021), 119538.
[25] J. Ran, J. Zhang, J. Yu, M. Jaroniec, S.Z. Qiao, Earth-abundant cocatalysts for semiconductor-based photocatalytic water splitting, Chem. Soc. Rev. 43 (2014) 7787–7812.
[26] Y. Wang, M. Zhou, Y. He, Z. Zhou, Z. Sun, In situ loading CuO quantum dots on TiO_2 nanosheets as cocatalyst for improved photocatalytic water splitting, J. Alloy. Compd. 813 (2020), 152184.
[27] Z.U. Rahman, N. Wei, M. Feng, D. Wang, TiO_2 hollow spheres with separated Au and RuO_2 co-catalysts for efficient photocatalytic water splitting, Int. J. Hydrogen Energy 44 (2019) 13221–13231.
[28] N. Rozman, P. Nadrah, R. Cornut, B. Jousselme, M. Bele, G. Dražić, M. Gaberšček, Š. Kunej, A.S. Škapin, TiO_2 photocatalyst with single and dual noble metal co-catalysts for efficient water splitting and organic compound removal, Int. J. Hydrogen Energy 46 (2021) 32871–32881.
[29] L. Yang, P. Gao, J. Lu, W. Guo, Z. Zhuang, Q. Wang, W. Li, Z. Feng, Mechanism analysis of Au, Ru noble metal clusters modified on TiO_2 (101) to intensify overall photocatalytic water splitting, RSC Adv. 10 (2020) 20654–20664.
[30] N. Ramesh Reddy, M. Mamatha Kumari, K.K. Cheralathan, M.V. Shankar, Enhanced photocatalytic hydrogen production activity of noble metal free MWCNT-TiO_2 nanocomposites, Int. J. Hydrogen Energy 43 (2018) 4036–4043.
[31] Q. Yue, Y. Wan, Z. Sun, X. Wu, Y. Yuan, P. Du, MoP is a novel, noble-metal-free cocatalyst for enhanced photocatalytic hydrogen production from water under visible light, J. Mater. Chem. A 3 (2015) 16941–16947.
[32] Y.J. Yuan, H.W. Lu, Z.T. Yu, Z.G. Zou, Noble-metal-free molybdenum disulfide cocatalyst for photocatalytic hydrogen production, ChemSusChem 8 (2015) 4113–4127.
[33] D. Kong, J.J. Cha, H. Wang, H.R. Lee, Y. Cui, First-row transition metal dichalcogenide catalysts for hydrogen evolution reaction, Energy Environ. Sci. 6 (2013) 3553–3558.
[34] J. Li, P. Jiménez-Calvo, E. Paineau, M.N. Ghazzal, Metal chalcogenides based heterojunctions and novel nanostructures for photocatalytic hydrogen evolution, Catalysts 10 (2020) 89.
[35] V. Navakoteswara Rao, P. Ravi, M. Sathish, M. Vijayakumar, M. Sakar, M. Karthik, S. Balakumar, K.R. Reddy, N.P. Shetti, T.M. Aminabhavi, M.V. Shankar, Metal chalcogenide-based core/shell photocatalysts for solar hydrogen production: recent advances, properties and technology challenges, J. Hazard. Mater. 415 (2021), 125588.
[36] Z. Ran, C. Shu, Z. Hou, L. Cao, R. Liang, J. Li, P. Hei, T. Yang, J. Long, Ni_3Se_2/$NiSe_2$ heterostructure nanoforests as an efficient bifunctional electrocatalyst for high-capacity and long-life Li–O_2 batteries, J. Power Sources 468 (2020), 228308.
[37] R.A. Hussain, I. Hussain, Fabrication and applications of nickel selenide, J. Solid State Chem. 277 (2019) 316–328.
[38] W. Guo, Q. Van, Le Do H.H., A. Hasani, M. Tekalgne, Ni_3Se_4@$MoSe_2$ composites for hydrogen evolution reaction, Appl. Sci. 9 (2019) 1–10.
[39] N. Moloto, M.J. Moloto, N.J. Coville, S. Sinha Ray, Optical and structural characterization of nickel selenide nanoparticles synthesized by simple methods, J. Cryst. Growth 311 (2009) 3924–3932.
[40] S. Wu, Q. Hu, L. Wu, J. Li, H. Peng, Q. Yang, One-step solvothermal synthesis of nickel selenide nanoparticles as the electrode for high-performance supercapacitors, J. Alloy. Compd. 784 (2019) 347–353.
[41] S. Mani, S. Ramaraj, S.M. Chen, B. Dinesh, T.W. Chen, Two-dimensional metal chalcogenides analogous $NiSe_2$ nanosheets and its efficient electrocatalytic performance towards glucose sensing, J. Colloid Interface Sci. 507 (2017) 378–385.
[42] L. Zhu, Q. Lu, L. Lv, Y. Wang, Y. Hu, Z. Deng, Z. Lou, Y. Hou, F. Teng, Ligand-free rutile and anatase TiO_2 nanocrystals as electron extraction layers for high performance inverted polymer solar cells, RSC Adv. 7 (2017) 20084–20092.
[43] Y. lang Cen, J. jie Shi, M. Zhang, M. Wu, J. Du, W. hui Guo, Y. hui Zhu, Optimized band gap and fast interlayer charge transfer in two-dimensional perovskite oxynitride Ba_2NbO_3N and Sr_2NbO_3/Ba_2NbO_3N bonded heterostructure visible-

light photocatalysts for overall water splitting, J. Colloid Interface Sci. 546 (2019) 20–31.
[44] Q. Chen, J. Zhang, J. Lu, H. Liu, Noble metal-free $NiSe_2$ nanosheets decorated MIL-53(Fe) microrods with highly efficient visible-light driven photocatalytic H_2 generation, Int. J. Hydrogen Energy 44 (2019) 16400–16410.
[45] G. Wang, Z. Jin, Function of $NiSe_2$ over CdS nanorods for enhancement of photocatalytic hydrogen production — from preparation to mechanism, Appl. Surf. Sci. 467–468 (2019) 1239–1248.
[46] L. Lai, F. Xing, C. Cheng, C. Huang, Hierarchical 0D $NiSe_2$/2D $ZnIn_2S_4$ nanosheet-assembled microflowers for enhanced photocatalytic hydrogen evolution, Adv. Mater. Interfaces 8 (2021) 0–7.
[47] H. Liu, T. Yan, Z. Jin, Q. Ma, Efficient photocatalytic hydrogen production by $Mn_{0.05}Cd_{0.95}S$ nanoparticles anchored on cubic $NiSe_2$, New J. Chem. 44 (2020) 14879–14889.
[48] H.Y. Hafeez, S.K. Lakhera, S. Bellamkonda, G.R. Rao, M.V. Shankar, D. W. Bahnemann, B. Neppolian, Construction of ternary hybrid layered reduced graphene oxide supported g-C_3N_4-TiO_2 nanocomposite and its photocatalytic hydrogen production activity, Int. J. Hydrogen Energy 43 (2018) 3892–3904.
[49] D. Joubert, From ultrasoft pseudopotentials to the projector augmented-wave method, Phys. Rev. B - Condens. Matter Mater. Phys. 59 (1999) 1758–1775.
[50] P.E. Blöchl, Projector augmented-wave method, Phys. Rev. B 50 (1994) 17953–17979.
[51] J.P. Perdew, J.A. Chevary, S.H. Vosko, K.A. Jackson, M.R. Pederson, D.J. Singh, C. Fiolhais, Special points for Brillonin-zone integrations*, Phys. Rev. B 48 (1993) 4978.
[52] X. Jaramillo-Fierro, L.F. Capa, F. Medina, S. González, Dft study of methylene blue adsorption on $ZnTiO_3$ and TiO_2 surfaces (101), Molecules 26 (2021) 3780.
[53] X. Teng, J. Wang, L. Ji, Y. Lv, Z. Chen, Ni nanotube array-based electrodes by electrochemical alloying and de-alloying for efficient water splitting, Nanoscale 10 (2018) 9276–9285.
[54] M. Ismael, Highly effective ruthenium-doped TiO_2 nanoparticles photocatalyst for visible-light-driven photocatalytic hydrogen production, New J. Chem. 43 (2019) 9596–9605.
[55] B. Bharti, S. Kumar, H.N. Lee, R. Kumar, Formation of oxygen vacancies and Ti^{3+} state in TiO_2 thin film and enhanced optical properties by air plasma treatment, Sci. Rep. 6 (2016) 1–12.
[56] J. Kuang, Z. Xing, J. Yin, Z. Li, S. Tan, M. Li, J. Jiang, Q. Zhu, W. Zhou, Ti^{3+} self-doped rutile/anatase/TiO_2(B) mixed-crystal tri-phase heterojunctions as effective visible-light-driven photocatalysts, Arab. J. Chem. 13 (2020) 2568–2578.
[57] Z. Chen, H. Gong, Q. Liu, M. Song, C. Huang, $NiSe_2$ nanoparticles grown in situ on CdS nanorods for enhanced photocatalytic hydrogen evolution, ACS Sustain. Chem. Eng. 7 (2019) 16720–16728.
[58] T. Hisatomi, J. Kubota, K. Domen, Recent advances in semiconductors for photocatalytic and photoelectrochemical water splitting, Chem. Soc. Rev. 43 (2014) 7520–7535.
[59] X. Guo, Y. Peng, G. Liu, G. Xie, Y. Guo, Y. Zhang, J. Yu, An efficient $ZnIn_2S_4$ @$CuInS_2$ core–shell p–n heterojunction to boost visible-light photocatalytic hydrogen evolution, J. Phys. Chem. C 124 (2020) 5934–5943.
[60] A.S. Malik, T. Liu, M. Dupuis, R. Li, C. Li, Water oxidation on TiO_2: a comparative DFT study of $1e^-$, $2e^-$, and $4e^-$ processes on rutile, anatase, and brookite, J. Phys. Chem. C 124 (2020) 8094–8100.
[61] A. Vittadini, A. Selloni, F.P. Rotzinger, M. Grätzel, Formic acid adsorption on dry and hydrated TiO_2 anatase (101) surfaces by DFT calculations, J. Phys. Chem. B 104 (2000) 1300–1306.
[62] S. Shen, H. Zhang, A. Xu, Y.Y. Zhao, Z. Lin, Z. Wang, W. Zhong, S. Feng, Construction of $NiSe_2$/$BiVO_4$ Schottky junction derived from work function discrepancy for boosting photocatalytic activity, J. Alloy. Compd. 875 (2021), 160071.
[63] A. Subrahmanyam, K.P. Biju, P. Rajesh, K. Jagadeesh Kumar, M. Raveendra, Kiran, Surface modification of sol gel TiO_2 surface with sputtered metallic silver for Sun light photocatalytic activity: initial studies, Sol. Energy Mater. Sol. Cells 101 (2012) 241–248.
[64] V. Kumaravel, M.D. Imam, A. Badreldin, R.K. Chava, J.Y. Do, M. Kang, A. Abdel-Wahab, Photocatalytic hydrogen production: role of sacrificial reagents on the activity of oxide, carbon, and sulfide catalysts, Catalysts 9 (2019) 276.
[65] D. Gogoi, A. Namdeo, A.K. Golder, N.R. Peela, Ag-doped TiO_2 photocatalysts with effective charge transfer for highly efficient hydrogen production through water splitting, Int. J. Hydrogen Energy 45 (2020) 2729–2744.
[66] W. Hao, L. Zhao, X. Li, L. Qin, S. Han, S.Z. Kang, Cu nanoclusters incorporated mesoporous TiO_2 nanoparticles: an efficient and stable noble metal-free photocatalyst for light driven H_2 generation, Int. J. Hydrogen Energy 46 (2021) 6461–6473.
[67] J.X. Yang, W.B. Yu, C.F. Li, W. Da Dong, L.Q. Jiang, N. Zhou, Z.P. Zhuang, J. Liu, Z. Y. Hu, H. Zhao, Y. Li, L. Chen, J. Hu, B.L. Su, PtO nanodots promoting Ti_3C_2 MXene in-situ converted Ti_3C_2/TiO_2 composites for photocatalytic hydrogen production, Chem. Eng. J. 420 (2021), 129695.
[68] T. Su, Z.D. Hood, M. Naguib, L. Bai, S. Luo, C.M. Rouleau, I.N. Ivanov, H. Ji, Z. Qin, Z. Wu, Monolayer $Ti_3C_2T_x$ as an effective co-catalyst for enhanced photocatalytic hydrogen production over TiO_2, ACS Appl. Energy Mater. 2 (2019) 4640–4651.
[69] D. Ramírez-Ortega, D. Guerrero-Araque, P. Acevedo-Peña, E. Reguera, H. A. Calderon, R. Zanella, Enhancing the photocatalytic hydrogen production of the ZnO–TiO_2 heterojunction by supporting nanoscale Au islands, Int. J. Hydrogen Energy 46 (2021) 34333–34343.
[70] T. Wei, Y.N. Zhu, X. An, L.M. Liu, X. Cao, H. Liu, J. Qu, Defect modulation of Z-scheme TiO_2/Cu_2O photocatalysts for durable water splitting, ACS Catal. 9 (2019) 8346–8354.
[71] L. Wang, G. Tang, S. Liu, H. Dong, Q. Liu, J. Sun, H. Tang, Interfacial active-site-rich 0D Co_3O_4/1D TiO_2 p-n heterojunction for enhanced photocatalytic hydrogen evolution, Chem. Eng. J. 428 (2022), 131338.
[72] M. Liu, L.-Z. Qiao, B.-B. Dong, S. Guo, S. Yao, C. Li, Z.-M. Zhang, T.-B. Lu, Photocatalytic coproduction of H_2 and industrial chemical over MOF-derived direct Z-scheme heterostructure, Appl. Catal. B Environ. 273 (2020), 119066.
[73] L. Zhong, B. Mao, M. Liu, M. Liu, Y. Sun, Y.T. Song, Z.M. Zhang, T.B. Lu, Construction of hierarchical photocatalysts by growing $ZnIn_2S_4$ nanosheets on Prussian blue analogue-derived bimetallic sulfides for solar co-production of H2 and organic chemicals, J. Energy Chem. 54 (2021) 386–394.